The Protein Journal (2020) 39:671–680
https://doi.org/10.1007/s10930-020-09938-5

Studying the Role of a Single Mutation of a Family 11 Glycoside Hydrolase Using High-Resolution X-ray Crystallography

Zhihong Li[1] · Xiaoshuai Zhang[1] · Chunran Li[1] · Andrey Kovalevsky[2] · Qun Wan[1]

Accepted: 26 October 2020 / Published online: 31 October 2020

Abstract
XynII is a family 11 glycoside hydrolase that uses the retaining mechanism for catalysis. In the active site, E177 works as the acid/base and E86 works as the nucleophile. Mutating an uncharged residue (N44) to an acidic residue (D) near E177 decreases the enzyme's optimal pH by ~ 1.0 unit. D44 was previously suggested to be a second proton carrier for catalysis. To test this hypothesis, we abolished the activity of E177 by mutating it to be Q, and mutated N44 to be D or E. These double mutants have dramatically decreased activities. Our high-resolution crystallographic structures and the microscopic pK_a calculations show that D44 has similar position and pK_a value during catalysis, indicating that D44 changes electrostatics around E177, which makes it prone to rotate as the acid/base in acidic conditions, thus decreases the pH optimum. Our results could be helpful to design enzymes with different pH optimum.

Keywords Glycoside hydrolase · pH-dependent activity · X-ray crystallography · Mutagenesis · Electrostatics · General acid/base catalysis

1 Introduction

Glycoside hydrolases (GHs) are widely used in drug, food, feed stock, paper pulp, and bioenergy industries [1–3], which break up the glycosidic bond in poly- or oligo-saccharides. XynII is a family 11 glycoside hydrolase (GH11) secreted by *Trichoderma reesei* fungus. The enzyme has a jellyroll-like structure composed of nine antiparallel β-strands and one α-helix, resembling the right hand palm. The secondary structure elements are termed the 'thumb', 'finger', and 'palm' regions, which are the typical characteristics of GH11 enzymes [4]. The XynII active site is located deeply in the palm region with xylose units spanning from the − 3 to the + 3 sites. After cleavage, the xylose units from the + 1 to the + 3 aglycan portion of the substrate are quickly released from the active site. The xylose units from the − 1 to the − 3 glycan sites are first attached to a catalytic residue (E86) in the active site and are released at the end of catalysis (Figure S1) [5]. XynII has been used as a model protein to study the classic retaining mechanism for GHs: One glutamate (E177) functions as the catalytic acid/base to break up the linkage between the − 1 and + 1 xylose units, whereas the other glutamate (E86) works as the nucleophile that attacks the glycosidic carbon to produce a glycosyl enzyme intermediate, which is quickly removed by an incoming water [6–8].

Xylanase has applications in different industries. In the paper industry, xylanase is used in the alkaline environment [9, 10]. While in the food and feed stock industries, the enzyme is used in the acidic environment [11, 12]. Thus, manipulating the pH optimum of xylanase by protein engineering has been a long goal to meet its industrial application. It is observed that xylanases with the optimal pH in the alkaline condition have a neutral (Asn) residue near the acid/base, while xylanases functioning in the acidic environment have an acidic residue (Asp) [13]. Thus, introducing a negatively charged residue close to the acid/base glutamate would decrease the pH optimum. For example, mutating the neutral residue (N35) near the acid/base glutamate (E172) of the *Bacillus circulans* xylanase (BCX) to aspartate

Electronic supplementary material The online version of this article (https://doi.org/10.1007/s10930-020-09938-5) contains supplementary material, which is available to authorized users.

✉ Qun Wan
qunwan@njau.edu.cn

[1] College of Science, Nanjing Agricultural University, Nanjing 210095, People's Republic of China

[2] Neutron Scattering Division, Oak Ridge National Laboratory, Oak Ridge, TN 37831, USA

decreased its pH optimum by about 1.0 unit [13]. It was proposed that the introduced aspartate (D35) would be protonated and work as the joint acid/base together with E172 to break up the glycosidic bond [13]. To test this hypothesis, we created several single or double mutants of XynII: N44D, N44D/E177Q, and N44E/E177Q. These mutants have significantly decreased activities and the pH optima were down shifted by ~ 1.0 unit compared to the native XynII. Our high-resolution X-ray crystallography shows that the overall structures of the mutants do not significantly change. In the N44D mutant, the altered electrostatics in the active site would change the rotation equilibrium of E177. At its optimal pH (pH 4.5), such rotation would reach the equilibrium to achieve its maximal activity. In the double mutants, D44 or E44 has changed the sugar configuration of the − 1 site xylose from the suitable $^4H_3$ configuration to other improper ones. Therefore, their activities are almost abolished.

2 Materials and Methods

2.1 Gene Cloning, Protein Expression And Purification

The gene of XynII present in *T. reesei* was synthesized and subcloned into the expression vector pET-NTMST. This vector contains the gene sequence of the 6 × His tag, the NusA protein as the fusion tag to enhance protein folding, and the TEV cleavage site (sequence: ENLYFQS) sequentially at the N terminus of XynII to express the fused protein [14]. Site-directed mutagenesis was conducted by synthesizing a primer containing a mutation and elongated by PCR using the wild type xylanase construct as the template. After sequence confirmation, the construct was amplified and purified.

The proteins were expressed with the BL21 (DE3) competent cells in the minimal media. After growing 4 ~ 6 h at 37 °C, the bacteria culture reached OD_{600} value of 0.6 ~ 0.8. After cooling down, 0.5 mM isopropyl β-D-1-thiogalactopyranoside (IPTG) was added to express the fusion protein at 18 °C for 12 h. The cells were centrifuged at 6000 × g for 30 min at 4 °C and stored at − 80 °C.

Approximately 10 g of wet cells were re-suspended in 50 mL lysis buffer (50 mM Tris-base pH 8.0, 1 mM DTT, 0.1 M PMSF, 400 mM NaCl, 5% glycerol) and were lysed with a high-pressure cell press (Union Co., People's Republic of China) at 4 °C. The cell suspension was clarified with centrifugation at 15,000 × g. The fused protein was initially purified by the immobilized metal affinity chromatography (IMAC) [15]. The supernatant was loaded to the Ni^{2+} affinity column. After washing, the protein was eluted with the gradient of 20 ~ 500 mM imidazole. The eluted protein was added with 1% (mass ratio) TEV and dialyzed overnight at 4 °C to cleave the fused NusA protein. The mixture was loaded to the nickel affinity column to retain NusA for the second step purification. The flow-through containing the cleaved xylanase was dialyzed against the Tris–HCl buffer (100 mM Tris, 100 mM NaCl, 1 mM dithiothreitol, pH 8.0) and concentrated to 30 mg mL^{-1}.

2.2 Steady State Enzyme Kinetics

Discontinuous assay of the xylanase activity was performed by quantitative determination of the reducing sugar concentration using the 3,5-dinitrosalicylic acid (DNS) reagent [16]: 1% bagasse xylan (w/w) was incubated at 50 °C for 5 min. When xylanase was added, the reaction was carried out at 50 °C for 8 min in the 100 mM NaAc buffer at pH5.0. After the reaction was terminated at 100 °C, the DNS reagent was added for color development. After cooling down to room temperature (25 °C), the color absorption was measured at the wavelength of 540 nm. The reducing sugar concentration was determined using the standard curve of D-xylose, and the enzyme catalytic rate was calculated. V_{max} values of WT and its variants were determined by fitting the nonlinear regression of the Michaelis – Menten – Henri equation using Origin 8.0 (OriginLab, USA).

2.3 Crystallization

Xylanase was crystallized using the hanging drop method in the following condition at 18 °C: 20% PEG 8000, 0.2 M NaI, 0.1 M MES-NaOH (pH 6.0) or 0.1 M NaAc (pH 4.5). We obtained the xylotriose bound state crystals by soaking the apo-state crystals into the stabilizing solution at pH 4.5 (25% PEG 8000, 0.2 M NaI, 0.1 M NaAc, 25% glycerol, pH 4.5) or pH 6.0 (25% PEG 8000, 0.2 M NaI, 0.1 M MES, 25% glycerol, pH 6.0) containing 250 mM xylotetraose. The soaking time varies from 5 to 30 min according to the crystal quality and ligand diffusion.

2.4 X-Ray Crystallography And Structure Analysis

Crystals were flash-frozen in liquid nitrogen for data collection. X-ray diffraction data were collected on the beam lines of BL18U1 and BL19U1 in the Shanghai Synchrotron Radiation Facility (SSRF) [17]. Data were processed using the HKL3000 program [18].

Structures were solved and refined using the program package Phenix [19]. The start model was obtained from PDB entry 2DFC with all waters and non-bonded ions removed [20]. After a few rounds of refinement using phenix.refine [21] interspersed with manual model building using the program Coot, the electron density of xylotriose was clearly visible in both the $2F_o-F_c$ and the F_o-F_c omit maps [22]. The ligand was incorporated into the F_o-F_c

electron density map according to its position for further refinement. The model quality was checked by the program MolProbity [23]. All protein figures were generated using the program Pymol (PyMOL Molecular Graphics System, Version 1.3, Schrödinger, LLC). All X-ray data collection, refinement statics, and the protein data bank deposited IDs are listed in Table S1–S3.

The distance difference matrix of C_α atoms of the X-ray structures was generated using the program DDMP {Richards, 1988 #76}. Accessible surface area of X-ray structures was analyzed using the program AreaIMol incorporated in the CCP4 suite {Winn, 2011 #77}. The xylose conformation and puckering parameters were calculated using an online web server (https://enzyme13.bt.a.u-tokyo.ac.jp/CP/) according to the Cremer – Pople formalism [24] and were compared with the dihedral angles of xylose units in xylan.

2.5 pK_a Calculations

We used the H^{++} web server (version 3.0) to calculate the microscopic pK_a values of the XynII mutants in the apo and X3 bound states [25]. The web server uses the Poisson–Boltzmann continuum electrostatics approach to approximate the electrostatic environment of biological macromolecules [25–28]. The pK_a calculations were carried out under the following condition: a salinity of 0.15 M, an internal dielectric constant of 10, an external dielectric constant of 80, and pH 4.5 (E177 in the downward conformation) or pH 6.0 (E177 in the upward conformation). For the apo and X3 bound states, their pK_a values were calculated according to their crystal structures. For the X6 bound state, the calculations were based on the E177Q-X6 structure (PDB: 4HK8) and mutated the corresponding residues to mimic the Michaelis–Menten complex structures.

3 Results

3.1 Kinetic Studies

Bagasse xylan was used as the substrate. The XynII activity *vs.* pH shows a bell-shaped profile. The optimal reaction pH values for WT, N44D, N44D/E177Q, and N44E/E177Q are 5.5, 4.5, 5.0, and 4.5, respectively (Fig. 1). The results show that mutating the uncharged asparagine (N44) near the acid/base (E177) to the acidic aspartate has decreased the optimal pH of xylan hydrolysis by ~ 1.0 unit. The activity of N44D has significantly decreased compared to WT. In the double mutants, E177 is substituted to Q and a new potential acid/base (D or E) is introduced in the active site at position 44. Because xylan is not homogeneous, K_m and k_{cat} values cannot be directly determined. Instead, we determined the Michaelis–Menten steady-state kinetic parameter, V_{max}, to characterize the activity of WT and the mutants at 50 °C and pH 5.0. The N44D, N44D/E177Q, and N44E/E177Q mutants only have 20%, 0.03%, and 0.03% activity compared with WT in the same condition (Table 1 and Figure S2).

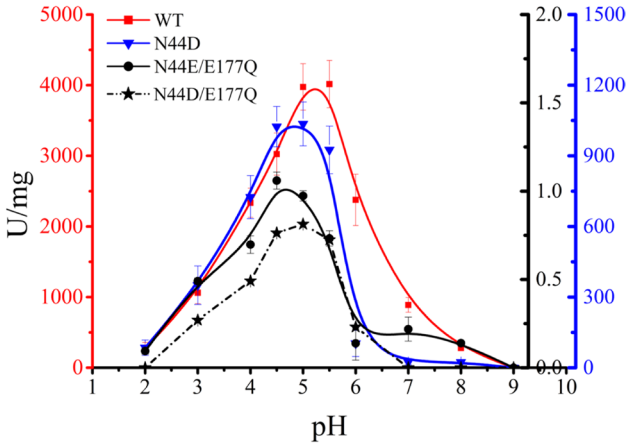

Fig. 1 The pH optima of WT, N44D, N44D/E177Q, N44E/E177Q. All these mutants have decreased their pH optima at pH 4.5 ~ 5.0. N44D has retained about 20% activity. N44D/E177Q and N44E/E177Q remain only about 0.03% activity compared with WT.

Table 1 Steady State Kinetic Parameters in the Discontinuous Assay

	Optimal pH	V_{max} (μmol min^{-1} mg^{-1}) [a]	Relative activity (%)
WT [b]	5.5	$(7.0 \pm 0.2) \times 10^3$	100
N44D	4.5	$(1.4 \pm 0.1) \times 10^3$	20
N44D/E177Q	5.0	1.8 ± 0.3	0.03
N44E/E177Q	4.5	2.1 ± 0.2	0.03

[a]Data were measured at pH 5.0 and 50 °C

[b]Data were extracted from our previous results [14]

3.2 X-ray Crystallography of N44D in the Apo and X3 Bound States

The crystal of N44D in the apo state at pH 6.0 has the space group of $P2_12_12_1$ and diffracted to 1.1 Å resolution and refined to 0.125 and 0.134 for R_{work} and R_{free}, respectively (Table S1). Comparing N44D and WT in the apo state (PDB: 2DFB), R.M.S.D. of C_α atoms between the two structures is only 0.13 Å, which indicates that mutating N44 to D does not incur large conformational change (Fig. 2a). Difference distance matrix (DDM) of the C_α atoms shows that the only significant changed regions are located in the finger loops (residues 20 ~ 23 and 40 ~ 45, Figure S3A). The WT structure was obtained in a different crystallization condition with a sulfate ion bound in this

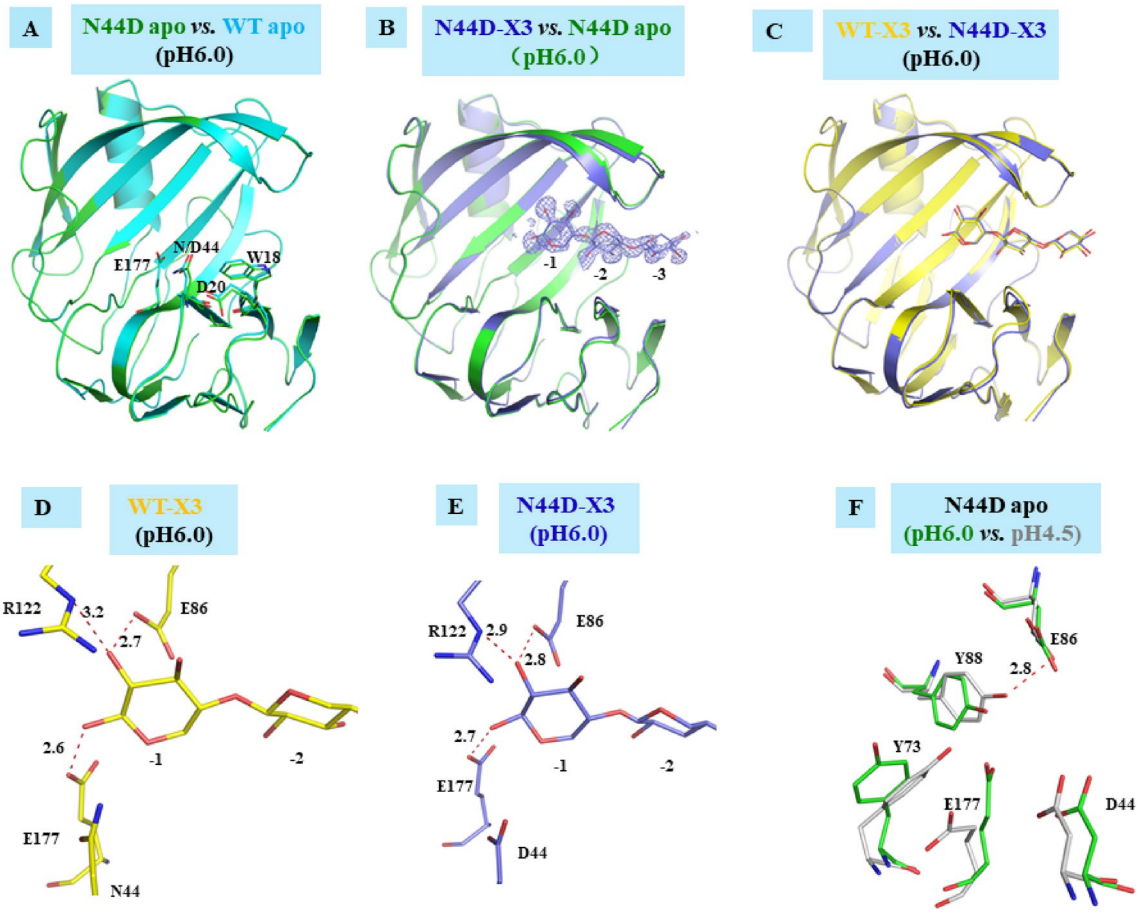

Fig. 2 Structural comparison among the WT and N44D. **a** Structural comparison between N44D and WT in the apo state at pH 6.0. **b** Structural comparison between the N44D-X3 state and the apo state at pH 6.0. **c** Structural comparison between the WT-X3 and the N44D-X3 states. **d** The close-up view of the active site of WT-X3 state. **e** The close-up view of the N44D-X3 state. **f** Comparison of the active sites of N44D between pH 6.0 and pH 4.5. All H-bond lengths are shown in Ångstroms

Table 2 Accessible surface area of WT and its mutants

	WT	N44D	N44D/E177Q	N44E/E177Q
Accessible surface area (Å^2)				
Overall	7956	7773	7848	7825
Active site	272	204	293	295
D/E44	–	28	42	57
E177	22.6	9.6	–	–

location, which probably causes the loop conformational difference (Figure S3B). The accessible surface area of E177 in the N44D mutant is significantly smaller than that of WT (Table 2). This N44D this mutation has increased negative charge in the active site. The distance between the carboxyl side chain of D44 and E177 in the mutant is 4.8 Å. In contrast, the distance between the amide side chain of N44 and the carboxyl side chain of E177 in WT is 4.4 Å. Likewise, W18 and D20 in N44D are slightly pushed away from D44 to accommodate the additional charge.

The N44D mutant has decreased ~ 80% activity compared to WT at their respective pH optima (Fig. 1). When we soaked xylotetraose (X4) into the apo state crystals, we only observed the hydrolyzed product, xylotriose (X3), spanning from the − 1 to the − 3 xylose-binding sites (Fig. 2b). The apo state and the X3 bound state structures are very similar (R.M.S.D. of C_α atoms is only 0.31 Å). Their major conformational changes occur in the 'thumb', the 'finger', and part of the 'palm' regions, which are consistent with our previous results when X3 was introduced into the apo state crystals of WT, Y77F, and Y88F mutants [5, 14]. Comparing the N44D-X3 and WT-X3 structures, they are very similar (R.M.S.D. of C_α atoms is only 0.26 Å). Even in the active site, there are no significant changes (Fig. 2c). In the WT-X3 structure, the OE1 atom of E86 has an H-bond (2.7 Å) with the O2B atom of the − 1 site xylose. The OE1 atom of E177 has an

H-bond (2.6 Å) with the O4A atom of the − 1 site xylose. The NE atom of Arg122 has a weak H-bond (3.2 Å) with the O2B atom of the − 1 site xylose (Fig. 2d and Figure S4A). In the N44D-X3 structure, the OE1 atom of E86 has an H-bond (2.8 Å) with the O2B atom of the -1 site xylose. The OE1 atom of E177 has an H-bond (2.7 Å) with the O4A atom of the -1 site xylose (Fig. 2e and Figure S4B). Thus, the configurations of the three xyloses in the N44D-X3 structure are the same as those in WT-X3 (Table 3). Specifically, the -1 site xylose has a conformation between $^4C_1$ and $^4H_3$, which indicates that GH11 has the $^1S_3 \rightarrow {}^4H_3 \rightarrow {}^4C_1$ pathway for hydrolysis [29].

To further analyze the function of D44 and E177 of the N44D mutant in the acidic environment, we crystallized the mutant at pH 4.5. The crystal has a new space group of I222 and diffracted to 1.2 Å, and the structure was refined to 0.158 and 0.169 for R_{work} and R_{free}, respectively (Table S2). The structure at pH 4.5 is similar with that at pH 6.0 (R.M.S.D. of C_α atoms is 0.68 Å). Interestingly, E177 moves downward and breaks up the original H-bond with Y88, which is consistent with our previous result when the WT crystal was in in the acidic condition at pH 4.4 [6]. As a result, the hydroxyl side chain of Y88 moves towards E86 and forms an H-bond (2.8 Å) with the carboxyl group of E86. Y77 also moves away from E86 and does not form any H-bond with E86. Y73 moves away from E177 to avoid electrostatic repulsion with the rotated E177. The position of D44 does not significantly change (Fig. 2f).

When we soaked X4 into the N44D crystal at pH 4.5, we obtained an N44D-X3 complex structure. Overall, the N44D-X3 and N44D apo state structures at pH 4.5 are very similar (R.M.S.D. of C_α atoms is only 0.21 Å). E177 is in the downward conformation in the presence of X3, which is consistent in the apo state at pH4.5. It indicates that the bound ligand would not affect the conformation of E177, and the acidic environment is the only cause to make E177 rotate.

3.3 X-ray Crystallography of N44D/E177Q in the Apo and X3 Bound States

To elucidate the role of D44, we mutated E177 to Q, which nullifies its catalytic property as the proton carrier. The crystal structures of N44D/E177Q and WT at pH 6.0 in the apo state are very similar (R.M.S.D. of C_α atoms is only 0.17 Å) (Fig. 3a). DDM of C_α atoms shows some local changes in the finger region, which is probably caused by sulfate binding and is consistent with the comparison between WT and N44D (Figure S3C). The accessible surface area of D44 in the N44D/E177Q mutant is significantly larger than E177 in WT (Table 2). The mutated Q177 in N44D/E177Q has almost the same position as E177 in WT. The distance of the carboxyl group of D44 to the amide group of Q177 is

Table 3 Xylose Parameters in the Xylanase-X3 Complexes

	Puckering parameters			Configuration	Dihedral angle [a]	
	Φ (°)	Θ (°)	Q (Å)		φ (°)	ψ (°)
WT-X3[b]						
− 3	270	177	0.60	$^4C_1$	− 85	163
− 2	202	174	0.57	$^4C_1$	− 103	157
− 1	194	160	0.52	**$^4C_1$/$^4H_3$**		
N44D-X3						
− 3	192	175	0.57	$^4C_1$	− 91	168
− 2	120	170	0.56	$^4C_1$	− 105	150
− 1	203	160	0.52	**$^4C_1$/$^4H_3$**		
N44D/E177Q-X3						
− 3	20	178	0.57	$^4C_1$	− 95	172
− 2	199	176	0.55	$^4C_1$	− 81	154
− 1	260	178	0.65	**$^4C_1$**		
N44E/E177N-X3						
− 3	223	179	0.60	$^4C_1$	− 88	166
− 2	190	170	0.58	$^4C_1$	− 105	154
− 1	178	163	0.53	**$^4C_1$**		
N44E/E177Q-X3						
− 3	256	175	0.57	$^4C_1$	− 85	168
− 2	169	171	0.60	$^4C_1$	− 95	144
− 1	216	142	0.57	**^4E**		

[a]The dihedral angles are defined as follows: φ, $O_{5i} - C_{1i} - O4_{i+1} - C4_{i+1}$; ψ, $C1_i - O4_{i+1} - C4_{i+1} - C3_{i+1}$

[b]Data were extracted from our previous results [14]

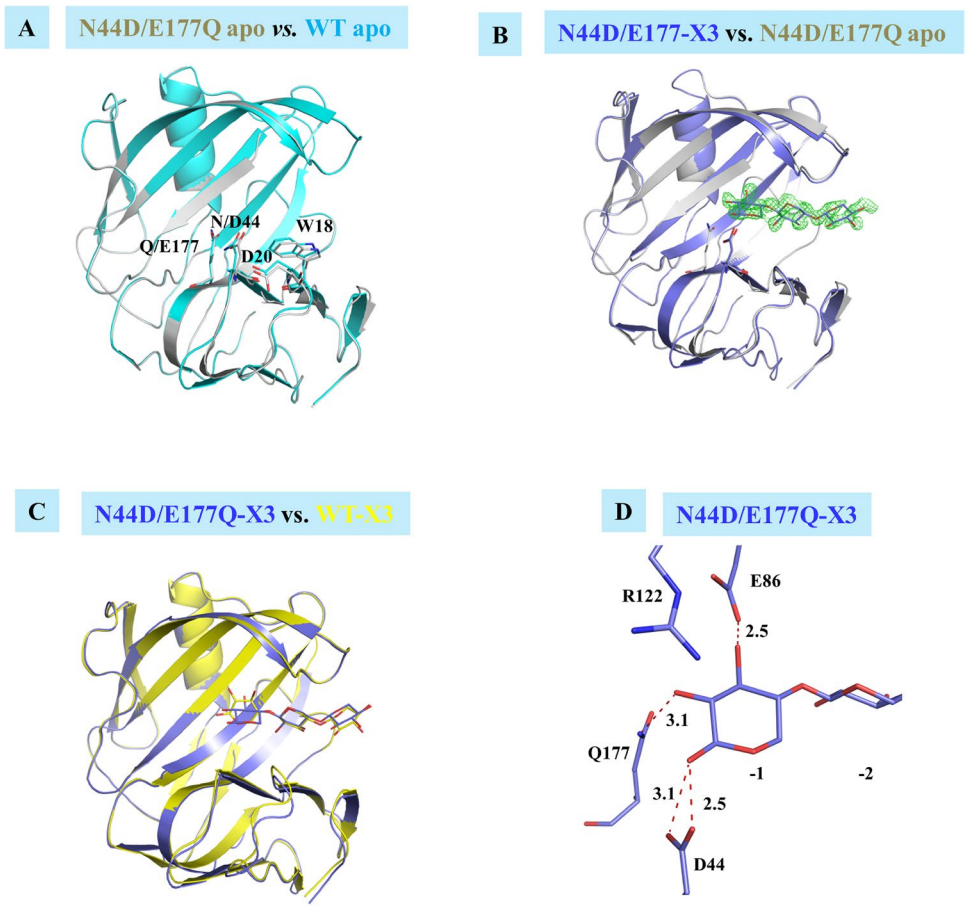

Fig. 3 Structural Comparison between N44D/E177Q and WT at pH 6.0. **a** Structural comparison between N44D/E177Q and WT in the apo state. **c** Structural comparison of N44D/E177Q between the X3 bound state and the apo state. The F_o−F_c omit map of X3 were contoured at 3 σ. **d** Structural comparison between the N44D/E177Q-X3 complex and the WT-X3 complex. **e** The H-bond interactions in the active site of N44D/E177Q-X3. All H-bond lengths are shown in Ångstroms

4.8 Å, which is a little longer than the distance between the amide group of N44 and the carboxyl group of E177 in WT (4.0 Å). D20 and W18 in N44D/E177Q move slightly away from D44 to adapt to the additional charge. The above subtle changes are consistent with the changes when we compare the structures of D44 and WT in the apo state. In this double mutant, there is an extra negative charge at the position of D44, but no charge at the position of Q177.

The N44D/E177Q mutant has only 0.03% activity compared to WT (Table 1). After soaking X4 in the apo state crystal at pH 6.0 for 5 min, we obtained X3 spanning from the − 3 to the − 1 xylose-binding sites (Fig. 3b). The N44D/E177Q-X3 structure is very similar to its apo state structure (R.M.S.D. of C_α atoms is only 0.20 Å). The only conformational changes are located in the thumb and part of the palm region, which is consistent with our previous soaking experiments [14]. The N44D/E177Q-X3 structure is also similar to the WT-X3 structure (R.M.S.D. of C_α atoms is only 0.31 Å) (Fig. 3c). However, there are significant conformational changes between the − 1 site xylose and its nearby residues in the active site. In the N44D/E177Q-X3 structure, there is a strong H-bond (2.5 Å) between the OE2 atom of E86 and the O3B atom of the − 1 site xylose. There is a weak H-bond (3.1 Å) between the NE2 atom of Q177 and the O2B atom of this xylose. The carboxyl group of D44 has a strong H-bond (2.5 Å) with the O4A atom of the − 1 site xylose. Arg122 is far away (4.4 Å) from the − 1 xylose (Figure S4C). Thus, it does not form an H-bond with this xylose unit (Fig. 3d). The configuration of the -1 site xylose in the double mutant is $^4C_1$ (Table 3).

3.4 X-ray Crystallography of N44E/E177Q in the Apo and X3 Bound States

The side chain of aspartate residue is shorter than that of glutamate and may not be a good proton carrier in XynII. Thus, we mutated N44 to E and E177 to Q, respectively, to investigate the role of E44 in N44E/E177Q. This double mutant retains only about 0.03% activity compared with WT (Table 1). The result indicates that E44 is a very poor proton carrier.

The apo state structure of N44E/E177Q at pH 6.0 is almost identical with the apo state structure of WT (The RMSD of C_α atoms is only 0.10 Å). DDM of C_α atoms shows some local changes in the finger region, which is consistent with the comparison between WT and N44D (Figure S3D). The accessible surface area of E44 in the N44E/E177Q mutant is significantly larger than E177 in

WT (Table 2). Q177 in the double mutant has very similar position compared with E177 in WT. The side chain of the mutated E44 has a different rotameric orientation compared with N44 in WT. To adapt to the subtle differences, D20 and W18 have slightly moved away (Fig. 4a). After soaking the apo state crystal with X4 for 5 min, we observed X3 bound in the active site. The 'thumb' region, the 'finger' region and part of the 'palm' region are attracted towards the bound oligosaccharide (Fig. 4b). In the active site, the O4A atom of the -1 site xylose has two H-bonds (2.5 Å and 3.0 Å) with the OH atom of Y88 and the NE2 atom of Q177, respectively. The O2B atom of the -1 site xylose has two H-bonds (2.7 Å and 2.8 Å) with the OE1 atom of E86 and the NE atom of R122, respectively. The O3B atom of the − 1 site xylose has a H-bond (2.6 Å) with the carbonyl oxygen of P126 (Fig. 4c and Figure S4D). Because of the different H-bond network, the -1 site xylose has the configuration of ^{4}E in the N44E/E177Q-X3 structure, which is unique among all the mutants (Table 3).

We also crystallized N44E/E177Q in the apo state at pH 4.5 (Table S3). The N44E/E177Q-X3 structure at pH 4.5 was obtained by soaking X4 into the active site for 18 min. The N44E/E177Q structures at pH 4.5 are similar with those at pH 6.0 (Figure S5A-S5B). The important residues (E44, E86 and E177) in the active site have almost the same positions in the different pH environments.

3.5 Microscopic p*K*a Calculations

We used the H^{++} web server which applies the Poisson–Boltzmann continuum electrostatics approach to calculate the microscopic p*K*a changes of D44 and E177 in N44D in the apo and the X3 bound states [25]. N44D is still catalytically active and cannot be co-crystallized with the substrates. We modeled the N44D-X6 complex structure by mutating Q177 to E and N44 to D using the E177Q-X6 structure (PDB: 4HK8) [5] as a starting model. In the WT apo state, E177 has the downward conformation at pH 4.4 (PDB ID: 4XQD), and the upward conformation at pH 6.0 (PDB ID: 4XPV) [6]. The structural changes of E177 in N44D are consistent with WT when pH changes. Nevertheless, D44 keeps the same position at both pH 4.5 and pH 6.0. Thus, we calculated the microscopic p*K*a values of E177 and D44 when E177 is in either the downward or the upward conformation (Table 4). The results show that the p*K*a value of E177 has significantly increased in the downward conformation, but decreased in the upward conformation. In contrast, the p*K*a values of D44 do not significantly change in both states. Our results indicate that E177 is still the major proton carrier, which adjusts its rotameric conformation to function as a base in its downward conformation and as an acid in its upward conformation.

4 Discussion

XynII from *T. reesei* is a typical family 11 glycoside hydrolase (GH11). Two catalytic glutamate residues function as the general acid/base and nucleophile. The side chain of E177 is proposed to rotate as an acid/base to break the glycosidic bond. Glu86 is hypothesized to work as the nucleophile to attack the glycosidic carbon to accelerate hydrolysis [4–6, 8, 30]. Some residues in the active site have interactions with E177, which could influence the equilibrium of E177 rotation, thus changes the optimal reaction pH [14]. Among these residues, N44 is particularly interesting. When it is mutated to D, the optimal reaction pH is decreased by ~ 1.0 unit. It was previously proposed that the mutated Asp and E177 would work as the joint acid/base for hydrolysis. Particularly, D44 could be an efficient acid/base per se [31, 32].

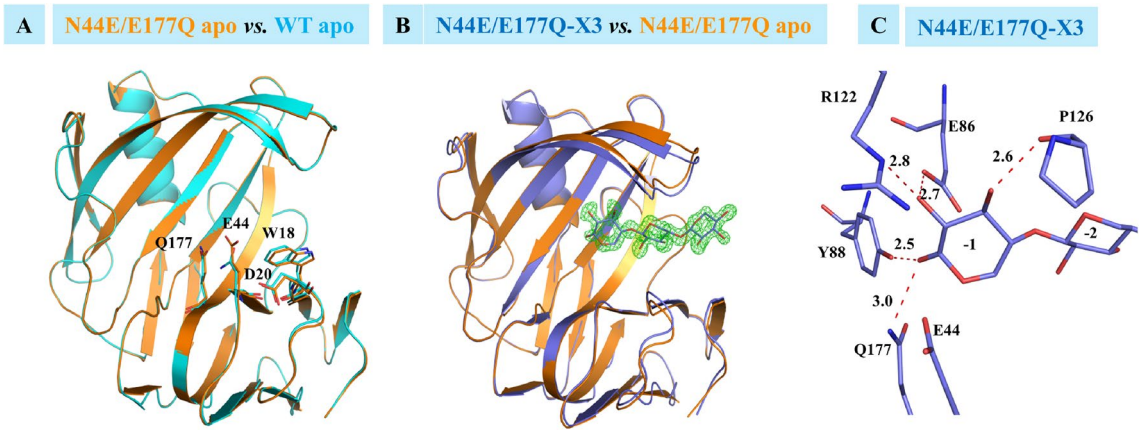

Fig. 4 Structural comparison between N44E/E177Q and WT at pH 6.0. **a** Structural comparison between N44E/E177Q and WT in the apo state. **b** Structural comparison of N44E/E177Q between the X3 bound state and the apo state. The $F_o - F_c$ omit map is contoured at 3σ. **c** The H-bond interactions in the active site of the N44E/E177Q-X3 complex. All H-bond lengths are shown in Ångstroms

Table 4 Calculated Microscopic pK_a Values of D44 and E177 in WT and the N44D Mutant

	WT			N44D					
	apo	X3	X6	apo		X3		X6	
	E177	E177	E177	D44	E177	D44	E177	D44	E177
Up	5.3	7.6	7.8	5.2	5.6	6.2	9.0	7.2	10.5
Down	6.0	8.9	8.5	4.8	8.3	6.4	9.5	7.3	> 12
ΔpK_a	+ 0.7	+ 1.3	+ 0.7	-0.4	+ 2.7	+ 0.2	+ 0.5	+ 0.1	> 1.5

Calculations for the X6 bound state structures were based on the crystal structure of the E177Q-X6 complex (PDB ID: 4HK8), but its Q177 was mutated back to the native E177 in WT. In the N44D-X6 complex, Q177 and N44 were mutated to E and D, respectively

Calculation parameters: salinity = 0.15, $\varepsilon_{int} = 10$, $\varepsilon_{ext} = 80$, pH 4.5 (downward) or pH 6.0 (upward)

To test this hypothesis, we studied the structures and functions of several mutants of XynII using enzyme kinetics, high-resolution X-crystallography, and microscopic pK_a calculations. Our results suggest that mutating N44 to D would change the electrostatic environment of E177, which can influence the equilibrium of E177 rotation for proton shuttling. Thus, the optimal reaction pH has been changed. However, the mutated Asp may not be an acid/base for direct catalysis.

Mutating N44 to D decreases the activity of XynII by about 70% ~ 80% (Table 1). We obtained the N44D-X3 structure by the soaking experiments at both pH 6.0 and pH 4.5, respectively. Comparing the structures of N44D with WT in the apo state and the X3 bound state at pH 6.0, they are very similar in the active site (Fig. 2). The Hydrogen bond (H-bond) network between X3 and its nearby interacting residues in N44D is also similar to that of WT. Thus, the configurations of all the xyloses in the active site in N44D are the same as those in WT: The configurations of the -2 and -3 site xyloses are $^4C_1$ and the configuration of the -1 site xylose is in the transition state between $^4C_1$ and $^4H_3$. QM/MM calculations indicate that when the oligoxylose is hydrolyzed, the -1 site xylose needs to be twisted and follow the pathway of $^1S_3 \rightarrow {}^4H_3 \rightarrow {}^4C_1$ for GH11 [29, 33]. Our results support this hypothesis.

Our X-ray crystallography structures show that D44 keeps a similar orientation when N44D was crystallized at both pH 4.5 and pH 6.0. In contrast, E177 has the downward conformation at pH 4.5 and the upward conformation at pH 6.0. The results are consistent in both the apo state and the X3 bound state (Fig. 2e), which suggests that E177 rotation is solely driven by pH changes, not by ligand binding. Neutron crystallography is a powerful tool to directly resolve the protonation states of residues, ligands and solvent in protein structures [34–36]. Our previous neutron crystallography structure of N44D at pH 5.8 (PDB ID: 4XPV) shows that both D44 and E177 are in the upward conformation without protonation. When WT was in the acidic environment (pH 4.4), E177 was protonated in the downward conformation (PDB ID: 4S2F) [6]. Thus, it is reasonable to propose that E177 in N44D might still be protonated in the downward conformation and unprotonated in the upward conformation. In other words, E177 still works as the proton carrier to break up the glycosidic bond. In comparison, D44 might not be a good proton carrier, which keeps the same orientation in different pH environments.

To investigate the role of D44 in N44D, we further abolished the function of E177 by mutating it to Q. The double mutant, N44D/E177Q, only has D44 as the proton carrier in the active site. The double mutant only retains 0.03% activity compared with WT, which indicates that D44 is a proton carrier with very low efficiency. The configuration of -1 site xylose is $^4C_1$, which is in the lowest energy state and makes the glycosidic bond difficult to be broken up [29]. The results could explain that even D44 is within the H-bond distance (2.5 Å) with the O4A atom, it cannot twist the -1 site xylose to the correct configuration for catalysis. Consequently, the activity of N44D/E177Q has been almost lost.

Aspartate has a shorter side chain than glutamate. Thus, D44 may not be a good substitute for E177 as the proton carrier. To better mimic the proton carrier at this residue position, we mutated N44 to E and abolished the function of E177 by mutating it to be Q. The double mutants, N44E/E177Q, has a similar structure with that of WT (Fig. 4). The two mutants retain only 0.03% ~ 0.04% activity compared with WT. These kinetic results show that E44 is a very inefficient proton carrier for catalysis. In the active site of the N44E/E177Q-X3 structure, the O4A atom of the -1 site xylose does not have any H-bond with E44. Instead, it has a strong H-bond (2.5 Å) with the hydroxyl group of Y88 (Fig. 4c). Together with other H-bonds with E86, R122, and P126, the -1 site xylose has the configuration of ^4E. The above results indicate that the configuration of the -1 site xylose can be diversified according to different H-bonds networks. However, when its configuration does not undergo the correct transition pathway [1, 35], the hydrolysis efficiency is dramatically decreased even though it is within the H-bond distance with a potential acid/base.

The accessible surface area of E177 in N44D is significantly smaller than that of WT. In contrast, the accessible

surface area of D44 or E44 in the other mutants is even larger than that of E177 in WT (Table 2). These results also indicate that D44 or E44 is not an ideal proton carrier as E177, thus, the activities of these mutants are significantly decreased.

We calculated the microscopic p*K*a values of E177 and D44 of N44D when E177 is in the upward or downward conformation. Though the absolute values from the p*K*a calculation might not be accurate, their differences (ΔpK_a) would indicate the p*K*a changes in different conformations [27]. The p*K*a values of D44 in different ligand-bound states do not significantly change. In comparison, the p*K*a value of E177 in the downward conformation is significantly higher than that of the upward conformation (Table 4). Thus, E177 should be the major proton carrier as the acid/base. When we compare the p*K*a values of N44D and WT in the upward conformation, the p*K*a values of E177 in the X3 and X6 bound states of N44D are significantly higher than those of the WT. The increased microscopic p*K*a would make E177 in N44D more difficult to release a proton as the acid. This result could explain why N44D has lower activity than WT.

Protein side-chain dynamics is within the picosecond to nanosecond range, while ligand binding and hydrolysis is within the microsecond to millisecond range [37]. Thus, it is reasonable to propose that when X6 binds in the active site, E177 has already picked up a proton in the solvent and ready to donate this proton as the general acid. In N44D, when the E177 side chain is upward, it is 4.7 Å away from the side chain of D44. When E177 rotates downward, it is 3.5 Å away from the D44 side chain. According to our calculation, the microscopic p*K*a of D44 is less than 5.0. Thus, in the neutral and alkaline pH, D44 is negatively charged, and E177 is prone to be in the upward conformation. In the acidic environment, D44 is protonated and neutral, thus, E177 would be easier to rotate downward with less electrostatic repulsion. At the optimal reaction pH (~pH 4.5), the rotation of E177 reaches the equilibrium to have the maximum activity. In summary, D44 has increased the negative charge around E177, which shifts the pH equilibrium and makes the mutant prone to function in a more acidic environment.

Bacillus circulans xylanase (BCX) is another well-studied GH11. When N35 in BCX (equivalent to N44 in XynII) is mutated to D, the activity is slightly increased as well as the pH optimum decreased [13, 31]. In the glycol-enzyme intermediate state of BCX (PDB ID: 1C5I), there is an H-bond between D35 and E172 (equivalent to E177 in XynII) [13]. When N35 is mutated to E and does not form any H-bond with E172, the activity of N35E decreases ~ 80% [31]. QM calculations demonstrate that when D35 is protonated, it forms a strong H-bond with E172, which decreases the activation energy for the glycosidic bond cleavage. Thus, this rate-limiting step has been enhanced [38]. In N44D of XynII, D44 is too far away to form an H-bond with E177 in either the apo state or the X3 bound state. Thus, the activity has been decreased. Our previous studies also demonstrate that the H-bond between Y88 and E177 is important to maintain the activity of XynII [14]. All these results highlight the importance of the H-bond formation between the acid/base and its neighboring residues, which would be suggestive for protein engineering to regulate both activity and pH optimum.

5 Conclusions

Our high-resolution X-crystallography structures show that the itinerary of $^{1}S_{3} \rightarrow {}^{4}H_{3} \rightarrow {}^{4}C_{1}$ is the proper pathway to break up the glycosidic bond. D44 in the N44D and the N44D/E177Q mutants is a very inefficient proton carrier for catalysis. One possible reason is that it could not appropriately regulate its p*K*a to deliver the proton as E177. The other possibility is that it cannot twist the -1 site xylose toward the correct intermediate state to break up the glycosidic bond. The major function of D44 in the N44D mutant is to change the equilibrium of E177 rotation as the proton carrier during catalysis. Our results could be helpful to design enzymes with different pH optimum by changing electrostatics around the catalytic residue.

Acknowledgements Q.W. was supported by the National Natural Science Foundation of China (No. 31670790), the Fundamental Research Funds for the Central Universities (No. KYXK202009), a Chinese Spallation Neutron Source User Special Grant, the Qing Lan Project of Jiangsu Province, and the Six Talent Peaks Project of Jiangsu Province. We thank the staff of the BL17U, BL18U1 and BL19U1 beamlines at Shanghai Synchrotron Radiation Facility, Shanghai, P.R. China, for assistance during X-ray data collection. Research at ORNL's HFIR and Spallation Neutron Source was sponsored by the Scientific User Facilities Division, Office of Basic Energy Sciences, U.S. Department of Energy.

Funding The authors declare no competing financial interest.

References

1. Payne CM, Knott BC, Mayes HB, Hansson H, Himmel ME, Sandgren M, Stahlberg J, Beckham GT (2015) Fungal Cellulases. Chem Rev 115:1308–1448
2. Speciale G, Thompson AJ, Davies GJ, Williams SJ (2014) Dissecting conformational contributions to glycosidase catalysis and inhibition. Curr Opin Struc Biol 28:1–13
3. Langan P, Gnanakaran S, Rector KD, Pawley N, Fox DT, Cho DW, Hammel KE (2011) Exploring new strategies for cellulosic biofuels production. Energ Environ Sci 4:3820–3833
4. Torronen A, Harkki A, Rouvinen J (1994) Three-dimensional structure of endo-1,4-beta-xylanase II from Trichoderma reesei: two conformational states in the active site. EMBO J 13:2493–2501
5. Wan Q, Zhang Q, Hamilton-Brehm S, Weiss K, Mustyakimov M, Coates L, Langan P, Graham D, Kovalevsky A (2014) X-ray

crystallographic studies of family 11 xylanase Michaelis and product complexes: implications for the catalytic mechanism. Acta Crystallogr SectD Biol Crystallogr. 70:11–23
6. Wan Q, Parks JM, Hanson BL, Fisher SZ, Ostermann A, Schrader TE, Graham DE, Coates L, Langan P, Kovalevsky A (2015) Direct determination of protonation states and visualization of hydrogen bonding in a glycoside hydrolase with neutron crystallography. Proc Natl Acad Sci USA 112:12384–12389
7. Vasella A, Davies GJ, Bohm M (2002) Glycosidase mechanisms. *Curr. Opin*. Chem Biol 6:619–629
8. Zechel DL, Withers SG (2000) Glycosidase mechanisms: Anatomy of a finely tuned catalyst. Acc Chem Res 33:11–18
9. Bai WQ, Cao YF, Liu J, Wang QH, Jia ZH (2016) Improvement of alkalophilicity of an alkaline xylanase Xyn11A-LC from Bacillus sp SN5 by random mutation and Glu135 saturation mutagenesis. BMC Biotechnol 16:77–86
10. Amel BD, Nawel B, Khelifa B, Mohammed G, Manon J, Salima KG, Farida N, Hocine H, Bernard O, Jean-Luc C, Marie-Laure F (2016) Characterization of a purified thermostable xylanase from Caldicoprobacter algeriensis sp nov strain TH7C1(T). Carbohydr Res 419:60–68
11. Polizeli MLTM, Rizzatti ACS, Monti R, Terenzi HF, Jorge JA, Amorim DS (2005) Xylanases from fungi: properties and industrial applications. Appl Microbiol Biotechnol 67:577–591
12. Fushinobu S, Ito K, Konno M, Wakagi T, Matsuzawa H (1998) Crystallographic and mutational analyses of an extremely acidophilic and acid-stable xylanase: biased distribution of acidic residues and importance of Asp37 for catalysis at low pH. Protein Eng 11:1121–1128
13. Joshi MD, Sidhu G, Pot I, Brayer GD, Withers SG, McIntosh LP (2000) Hydrogen bonding and catalysis: A novel explanation for how a single amino acid substitution can change the pH optimum of a glycosidase. J Mol Biol 299:255–279
14. Li ZH, Zhang XS, Wang QQ, Li CR, Zhang NY, Zhang XK, Xu BR, Ma BL, Schrader TE, Coates L, Kovalevsky A, Huang YD, Wan Q (2018) Understanding the pH-Dependent Reaction Mechanism of a Glycoside Hydrolase Using High-Resolution X-ray and Neutron Crystallography. ACS Catal 8:8058–8069
15. Bornhorst JA, Falke JJ (2000) Purification of proteins using polyhistidine affinity tags. Method Enzymol 326:245–254
16. Bailey MJ, B. P., Poutanen K., (1992) Interlaboratory testing of methods for assay of xylanase activity. J Biotechnol 23:257–270
17. Wang QS, Zhang KH, Cui Y, Wang ZJ, Pan QY, Liu K, Sun B, Zhou H, Li MJ, Xu Q, Xu CY, Yu F, He JH (2018) Upgrade of macromolecular crystallography beamline BL17U1 at SSRF. Nucl Sci Tech 29:68
18. Minor W, Cymborowski M, Otwinowski Z, Chruszcz M (2006) HKL-3000: the integration of data reduction and structure solution–from diffraction images to an initial model in minutes. Acta Crystallogr Sect D: Biol Crystallogr 62:859–866
19. Adams PD, Afonine PV, Bunkoczi G, Chen VB, Davis IW, Echols N, Headd JJ, Hung LW, Kapral GJ, Grosse-Kunstleve RW, McCoy AJ, Moriarty NW, Oeffner R, Read RJ, Richardson DC, Richardson JS, Terwilliger TC, Zwart PH (2010) PHENIX: a comprehensive Python-based system for macromolecular structure solution. Acta Crystallogr Sect D: Biol Crystallogr 66:213–221
20. Watanabe N, Akiba T, Kanai R, Harata K (2006) Structure of an orthorhombic form of xylanase II from Trichoderma reesei and analysis of thermal displacement. Acta Crystallogr Sect D: Biol Crystallogr 62:784–792
21. Afonine PV, Grosse-Kunstleve RW, Echols N, Headd JJ, Moriarty NW, Mustyakimov M, Terwilliger TC, Urzhumtsev A, Zwart PH, Adams PD (2012) Towards automated crystallographic structure refinement with phenix.refine. Acta Crystallogr Sect D Biol Crystallogr 68:352–367
22. Emsley P, Lohkamp B, Scott WG, Cowtan K (2010) Features and development of Coot. Acta Crystallogr Sect D: Biol Crystallogr 66:486–501
23. Chen VB, Arendall WB, Headd JJ, Keedy DA, Immormino RM, Kapral GJ, Murray LW, Richardson JS, Richardson DC (2010) MolProbity: all-atom structure validation for macromolecular crystallography. Acta Crystallogr Sect D: Biol Crystallogr 66:12–21
24. Jeffrey GA, Yates JH (1979) Stereographic Representation of the Cremer-Pople Ring-Puckering Parameters for Pyranoid Rings. Carbohydr Res 74:319–322
25. Anandakrishnan R, Aguilar B, Onufriev AV (2012) H++ 3.0 automating pK prediction and the preparation of biomolecular structures for atomistic molecular modeling and simulations. Nucleic Acids Res 40:537–541
26. Zhou HX, Pang XD (2018) Electrostatic Interactions in Protein Structure, Folding, Binding, and Condensation. Chem Rev 118:1691–1741
27. Sun ZX, Wang XH, Song JN (2017) Extensive Assessment of Various Computational Methods for Aspartate's pK(a) Shift. J Chem Inf Model 57:1621–1639
28. Cheng YS, Chen CC, Huang CH, Ko TP, Luo W, Huang JW, Liu JR, Guo RT (2014) Structural analysis of a glycoside hydrolase family 11 xylanase from Neocallimastix patriciarum: insights into the molecular basis of a thermophilic enzyme. J Biol Chem 289:11020–11028
29. Iglesias-Fernandez J, Raich L, Ardevol A, Rovira C (2015) The complete conformational free energy landscape of beta-xylose reveals a two-fold catalytic itinerary for beta-xylanases. Chem Sci 6:1167–1177
30. Rye CS, Withers SG (2000) Glycosidase mechanisms. Curr Opin Chem Biol 4:573–580
31. Ludwiczek ML, D'Angelo I, Yalloway GN, Brockerman JA, Okon M, Nielsen JE, Strynadka NCJ, Withers SG, McIntosh LP (2013) Strategies for Modulating the pH-Dependent Activity of a Family 11 Glycoside Hydrolase. Biochemistry 52:3138–3156
32. Joshi MD, Sidhu G, Nielsen JE, Brayer GD, Withers SG, McIntosh LP (2001) Dissecting the electrostatic interactions and pH-dependent activity of a family 11 glycosidase. Biochemistry 40:10115–10139
33. Ardevol A, Rovira C (2015) Reaction Mechanisms in Carbohydrate-Active Enzymes: Glycoside Hydrolases and Glycosyltransferases. Insights from ab Initio Quantum Mechanics/Molecular Mechanics Dynamic Simulations. J Am Chem Soc 137:7528–7547
34. Kwon H, Langan PS, Coates L, Raven EL, Moody PCE (2018) The rise of neutron cryo-crystallography. Acta Crystallogr Sect D: Struct Biol 74:792–799
35. Chen JCH, Unkefer CJ (2017) Fifteen years of the Protein Crystallography Station: the coming of age of macromolecular neutron crystallography. IUCrJ 4:72–86
36. O'Dell WB, Bodenheimer AM, Meilleur F (2016) Neutron protein crystallography: A complementary tool for locating hydrogens in proteins. Arch Biochem Biophys 602:48–60
37. Henzler-Wildman K, Kern D (2007) Dynamic personalities of proteins. Nature 450:964–972
38. Li JH, Wang LS (2011) Why substituting the asparagine at position 35 in Bacillus circulans xylanase with an aspartic acid remarkably improves the enzymatic catalytic activity? A quantum chemistry-based calculation study. Polym Degrad Stab 96:1009–1014